Journal of The Electrochemical Society

The Electrochemical Society
Advancing solid state & electrochemical science & technology

OPEN ACCESS

Ni_xSi_{1-x} Alloys Prepared by Mechanical Milling as Negative Electrode Materials for Lithium Ion Batteries

To cite this article: Zhijia Du *et al* 2016 *J. Electrochem. Soc.* **163** A13

View the article online for updates and enhancements.

ECS Membership = Connection

ECS membership connects you to the electrochemical community:

- Facilitate your research and discovery through ECS meetings which convene scientists from around the world;
- Access professional support through your lifetime career:
- Open up mentorship opportunities across the stages of your career;
- Build relationships that nurture partnership, teamwork—and success!

Join ECS! Visit electrochem.org/join

This content was downloaded from IP address 134.190.164.141 on 03/08/2022 at 13:55

Ni_xSi_{1-x} Alloys Prepared by Mechanical Milling as Negative Electrode Materials for Lithium Ion Batteries

Zhijia Du,[a,*] S. N. Ellis,[b] R. A. Dunlap,[a,c,d] and M. N. Obrovac[a,b,c,,z]**

[a]*Department of Physics and Atmospheric Science, Dalhousie University, Halifax, Nova Scotia B3H 4R2, Canada*
[b]*Department of Chemistry, Dalhousie University, Halifax, Nova Scotia B3H 4R2, Canada*
[c]*Institute for Research in Materials, Dalhousie University, Halifax, Nova Scotia B3H 4R2, Canada*
[d]*College of Sustainability, Dalhousie University, Halifax, Nova Scotia B3H 4R2, Canada*

Ni_xSi_{1-x} ($0 \leq x \leq 0.5$, $\Delta x = 0.05$) alloys were prepared by ball milling and studied as anode materials for lithium ion batteries. Nanocrystalline Si/$NiSi_2$ phases were formed for $x \leq 0.25$. The NiSi phase was observed for samples with higher Ni content. Increasing the Ni content was found to gradually lower the lithiation voltage, while delithiation voltage was not affected for $x \leq 0.25$. As a result, $Li_{15}Si_4$ did not form during cycling for $x > 0.15$. The capacity trend of Ni_xSi_{1-x} alloys with composition suggested that the nanocrystalline $NiSi_2$ phase had some activity toward Li, while the NiSi phase had no capacity toward Li. In situ XRD studies confirmed the activity of nanocrystalline $NiSi_2$. The best cycling performance of Ni_xSi_{1-x} alloys was obtained for $x = 0.20$ with 94% capacity retention after 50 cycles.

© The Author(s) 2015. Published by ECS. This is an open access article distributed under the terms of the Creative Commons Attribution Non-Commercial No Derivatives 4.0 License (CC BY-NC-ND, http://creativecommons.org/licenses/by-nc-nd/4.0/), which permits non-commercial reuse, distribution, and reproduction in any medium, provided the original work is not changed in any way and is properly cited. For permission for commercial reuse, please email: oa@electrochem.org. [DOI: 10.1149/2.0011602jes] All rights reserved.

Manuscript submitted September 4, 2015; revised manuscript received October 20, 2015. Published October 29, 2015.

Si-based anode materials for lithium-ion batteries have received considerable research effort because of their low cost and high volumetric capacity (2194 Ah/L for Si, compared to 764 Ah/L for graphite).[1] Taking the delithiation voltage into consideration, Si can theoretically provide ~34% energy density improvement over graphite in a full cell model.[2] However, the volume expansion of Si during lithiation can be as high as 280%.[3] This is detrimental to cycling performance because it can result in disruption of the solid electrolyte interphase and the loss of electrical contact among the active particles in an electrode.[4,5] Incorporating Li-inactive elements with Si to form active/inactive alloys is one promising approach to mitigate these problems. A specific design strategy for such alloys has been proposed which can achieve maximum volumetric energy density on the basis of the fact that their molar volume of lithium is independent of lithium content and that their average voltage is lower than that of pure Si for a given volume expansion.[1]

For pure Si, $Li_{15}Si_4$ can suddenly crystallize at ~50 mV.[3] It is suspected that the formation of $Li_{15}Si_4$ is related to poor cycle performance due to particle fracture caused by high stresses at a two-phase conversion front.[6] While the inactive phase in a Si alloy functions as a "bystander" with the function of diluting volume expansion, it has actually been found to modify voltage characteristics and thus the structural variation of Si during lithiation/delithiation.[2,7] In a recently published article, it was shown that the formation of $Li_{15}Si_4$ is avoided during cycling of 3 M V6 active/inactive Si alloy, even at lower cutoff voltages as low as a 5 mV.[8,9] The absence of $Li_{15}Si_4$ formation has been shown to result in improved cycling performance in alloys.[3]

Si-TM alloys (TM = a transition metal) have been extensively studied as negative electrodes. When made by sputtering or ball milling, such alloys typically form active Si / inactive matrix nanostructured composites, where the inactive matrix comprises a transition metal silicide.[3,7,10–21] Although transition metal silicides are theoretically active with lithium from a thermodynamic basis,[10] most have been found to be completely inactive or have very limited capacity at room temperature.[3,12–17] For instance, Fleischauer et al. used a model based on effective heats of formation to explain the capacity behavior of (Fe, Mn, Cr+Ni, Co)-Si alloys. Using this model, they predicted that these alloys were composed of an active Si phase co-existing with the inactive FeSi, MnSi, CrSi, NiSi or $CoSi_2$ phases. This well predicted the observed alloy capacities.[16,17] In contrast to the above studies, researchers have reported some silicides may have considerable lithiation capacity, especially Ni-Si intermetallic compounds in which either NiSi or $NiSi_2$ have been reported to be active with Si.[11,18–21]

Recently we have proposed a different model to explain the electrochemical behavior of Ni-Si thin films in terms of internal stresses between active and inactive phases.[7] It has been shown that applied stress can significantly affect the potential of the Si voltage curve during cycling.[22] In Si thin films, the presence of a fixed substrate results in compressive stress when the Si expands during lithiation. This results in lowering the Si lithiation voltage curve by as much as 200 mV, resulting in a reduction in capacity. We studied Ni-Si nanocrystalline/amorphous thin films prepared by combinatorial sputtering over a large composition range.[7] These alloys show that similar behavior as Si thin films, where the presence of the fixed volume inactive phase results in applied stress to the active Si phase as it expands during lithiation. However, an inactive phase in an alloy can apply considerably more stress to an active Si phase than a fixed substrate. This results in the lowering of the lithiation voltage. However, the delithiation voltage remained unaffected. We speculated that particle fracture can reduce tensile stress during delithiation, as has been suggested during the delithiation of thin films.[22] These results suggested that all Si in sputtered Ni-Si thin films were active and that the capacity decreases with increasing Ni content only because of the suppression of the Si lithiation voltage via stress-potential coupling between the active Si phase and inactive Ni phase. For Ni contents larger than 50 atomic percent, the Si voltage curve in Ni-Si films was lowered by such a large amount that it resided below zero volts and the alloy became inactive.

The different preparation methods used to make Ni-Si alloys in previous studies result in different microstructures, and are likely the cause of the disparate reaction mechanisms reported. Since powders are used in conventional electrode coatings, capacity-composition relationships obtained from nanocrystalline/amorphous thin films might not be applicable to powder-based conventional coatings in Li-ion batteries. In addition, TM-Si binary systems or Li-TM-Si ternary systems vary in their phase behavior, which can result in rather different electrochemical performance. Therefore, careful study of each alloy system made by different synthesis methods is necessary to fully understand Si-TM alloy behavior.

In the present paper, Ni_xSi_{1-x} ($0 \leq x \leq 0.5$, at $\Delta x = 0.05$ intervals) alloys were prepared by mechanical milling and were evaluated as anode materials for lithium ion batteries. The effect of structure and composition on the electrochemical performance of these alloys was determined.

*Electrochemical Society Student Member.
**Electrochemical Society Active Member.
[z]E-mail: mnobrovac@dal.ca

Experimental

Ni_xSi_{1-x} ($0 \leq x \leq 0.5$, $\Delta x = 0.05$) alloys were prepared by ball milling as described in Reference 23. The starting materials were Ni powder (Alfa Aesar, −325 mesh, typically 99.8%) and silicon powder (Sigma-Aldrich, −325 mesh, 99%). A total of 5 mL of Ni and Si powders together with 2.3 Kg 0.25 inch stainless steel balls were loaded into the ball milling vessels and sealed under argon atmosphere. The samples were ball milled for 4 weeks at a milling speed of about 100 rpm.

X-ray diffraction patterns were collected using a JD2000 diffractometer equipped with a Cu K_α X-ray source and a diffracted beam monochromator. Each XRD scan was collected from 10° to 80° 2-theta in 0.05° increments for 2 seconds per step. True sample densities were measured using a Micromeritics AccuPyc II 1340 gas pycnometer. Fe content was obtained using inductively coupled plasma optical emission spectroscopy (ICP-OES) (Teledyne Leeman Labs Prodigy high dispersion ICP-OES).

Electrode slurries were made by mixing Ni-Si alloys, graphite (SFG6L, Timcal), carbon black (from Super P, Erachem Europe) and a 10 weight % aqueous solution of lithium polyacrylate (LiPAA) with a volumetric ratio of 45/35/3/19 or 80/0/5/15 in distilled water. The mixing was conducted in a PM200 Planetary Ball Mill with 4 WC balls (the ball/sample weight ratio was 15:1) at 100 rpm for a period of 1 h. The slurries were coated on electrolytic Cu foil (Furukawa Electric, Japan) using a 0.004 inch gap coating bar and dried at 120°C in air for 1 h. Typical active material loadings were about 4.0 mg/cm^2. Electrodes containing graphite were then passed through an adjustable gap calender with 6″ diameter rolls (DPM Solutions, Nova Scotia, Canada) to lower the porosity to ∼25%.

Electrodes were assembled in 2325-type coin cells with a lithium foil counter/reference electrode. Two layers of Celgard 2300 separator were used in each coin cell. 1 M $LiPF_6$ (BASF) in a solution of ethylene carbonate, diethyl carbonate and monofluoroethylene carbonate (volume ratio 3:6:1, all from Novolyte Technologies) was used as electrolyte. Cell assembly was carried out in an Ar-filled glove box. Cells were cycled galvanostatically at 30.0 ± 0.1°C between 5 mV and 0.9 V using a Maccor Series 4000 Automated Test System at a C/10 rate for the 1st cycle and a C/5 rate for the following cycles with a C/20 trickle discharge (lithiation).

For the in-situ XRD study of a $Ni_{0.25}Si_{0.75}$ sample, the electrode slurry was coated onto one side of a beryllium disc and dried in air at 120°C for 1 hour. This electrode / Be window was then used to prepare a coin cell in an Ar-filled glove box using specialized coin cell hardware, as described in Reference 24. The cell was discharged or charged to desired voltage, as described above, and then XRD measurements were performed, also as described above.

Results and Discussion

The composition of the Si-Ni samples as measured by ICP-OES revealed a minor iron impurity of about 0.4 atomic percent. This small iron impurity is likely from the milling process and was considered to have little effect on structure or electrochemistry of the Ni-Si alloys. Figure 1a shows XRD patterns of the Ni_xSi_{1-x} samples for $0 \leq x \leq 0.25$ with peak locations and intensities indicated for Si (PDF No. 00-080-0018[25]) and $NiSi_2$ (PDF No. 96-900-9025[25]). The reference XRD patterns for Si and $NiSi_2$ have nearly identical peak positions. This makes it difficult to differentiate the two phases. However, the relative peak intensities differ for these phases, which can aid in their disambiguation. The X-ray pattern for pure Si after 4 weeks ball milling shows features of amorphous Si, with two broad peaks of approximately equal area near the three major Si peaks. With increasing Ni content, the broad peaks from amorphous Si reduce in intensity and are replaced with peaks from a new phase having more narrow peaks than the broad peaks of pure amorphous Si. This new phase has relative peak intensities that are the same as $NiSi_2$, with the $Ni_{0.25}Si_{0.75}$ sample having a (111):(220):(311) peak ratio of 40:49:11, which is close to the theoretical value of 40:48:12. Based on this evidence, we

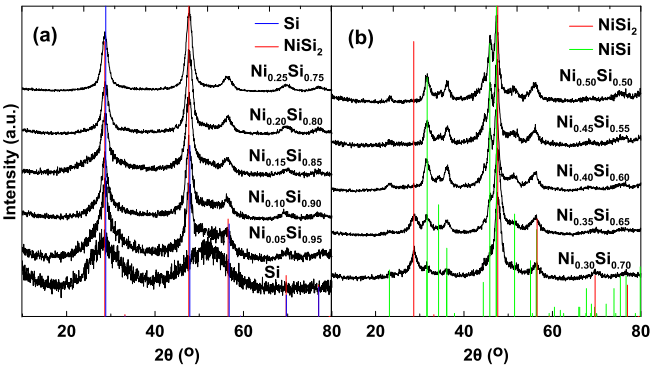

Figure 1. XRD patterns of ball milled Ni_xSi_{1-x} alloys: (a) $0 \leq x \leq 0.25$; (b) $0.30 \leq x \leq 0.50$. Vertical lines in the figure indicate known peak positions for Si, $NiSi_2$ and NiSi.

believe that $NiSi_2$ is progressively being formed as the Ni content is increased. As a result, the amount of elemental silicon phase present in the sample also decreases. The $NiSi_2$ phase thus formed has a grain size of about 3.5 nm, according to the Scherrer equation, and based on the (200) peak at 47.6° 2-theta.

Figure 1b shows XRD patterns of Ni_xSi_{1-x} alloys for $0.3 \leq x \leq 0.5$ with the peak positions and intensities of $NiSi_2$ and NiSi (PDF No. 00-085-0901[25]) indicated. Small NiSi peaks can be observed in $Ni_{0.30}Si_{0.70}$ sample. With further increase of Ni in the starting materials, the compositions enter the $NiSi_2$-NiSi two-phase region, as predicted by the equilibrium Ni-Si phase diagram, and, accordingly, the $NiSi_2$ phase gradually disappears with the evolution of the NiSi phase in the XRD patterns. Pure NiSi phase was formed for the composition with $x = 0.5$, also as predicted by the equilibrium Ni-Si phase diagram.

Figure 2 shows the voltage curves of selected Ni_xSi_{1-x} alloy electrodes. As the Ni content is increased, the alloy capacity decreases. Differential capacity curves of these electrodes are shown in Figure 3. The differential capacity curves are typical of amorphous Si, with two broad peaks during lithiation and delithiation. We have labeled these peaks A and B (during delithiation) and A′ and B′ (during lithiation), as indicated in Figure 3. It can be clearly seen that peak A and B shift to lower voltages with increasing x. This is a similar trend as observed with sputtered Ni-Si electrodes.[7] For $x \geq 0.35$, peak B is truncated at 0 V, resulting in capacity reduction. This makes the determination of the amount of active Si present difficult to determine from the cell capacity alone. As discussed in Ref. 6, the amount of active Si can be determined from the differential capacity by a peak fitting procedure. Therefore, peak-fitting was done in this study, as discussed below.

Si alloys have superior cycling characteristics when blended with graphite and calendered to about 25% porosity, as we suggest they would be used in practical lithium ion batteries.[9] Such coatings are

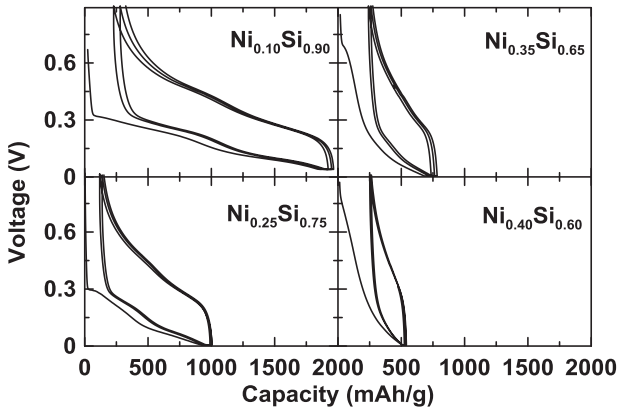

Figure 2. Voltage curves of $Ni_{0.10}Si_{0.90}$, $Ni_{0.25}Si_{0.75}$, $Ni_{0.35}Si_{0.65}$, $Ni_{0.40}Si_{0.60}$ alloy electrodes.

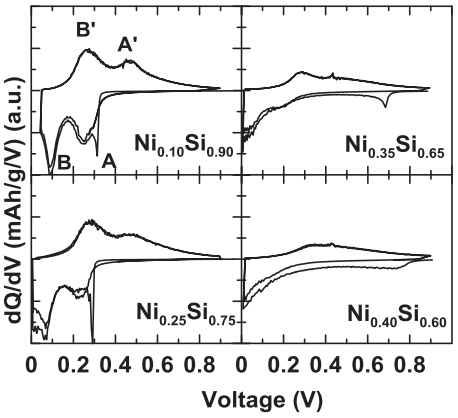

Figure 3. Differential capacity curves of $Ni_{0.10}Si_{0.90}$, $Ni_{0.25}Si_{0.75}$, $Ni_{0.35}Si_{0.65}$, $Ni_{0.40}Si_{0.60}$ alloy electrodes, with peaks labeled as defined in the text.

ideal for the evaluation of new alloy anode powders. Figure 4 shows voltage curves of calendered Ni–Si alloy–graphite electrodes. All the electrodes display sloping plateaus showing single-phase behavior, similar to that of amorphous silicon, and no $Li_{15}Si_4$ was formed during lithiation/delithiation for the first three cycles. Small plateaus at around 0.2 V during delithiation are ascribed to graphite. The capacity of the electrodes decreases with increasing x. The voltage curve for $Ni_{0.50}Si_{0.50}$-graphite composite electrodes only shows voltage features of graphite, indicating that the $Ni_{0.50}Si_{0.50}$ sample is completely inactive toward Li.

In a previous study of sputtered Ni-Si thin films, we showed that the lithiation voltage is depressed with increasing Ni content, while the delithiation voltage remains unchanged.[7] Figure 5 shows the average second lithiation/delithiation voltage of Ni_xSi_{1-x} alloys as a function of composition, calculated for the cells shown in Figure 4 by subtracting the contribution of graphite. It is clearly seen that the average lithiation voltage is continuously depressed by increasing x. Meanwhile, the delithiation voltage shows little change for $x \leq 0.25$ and starts to

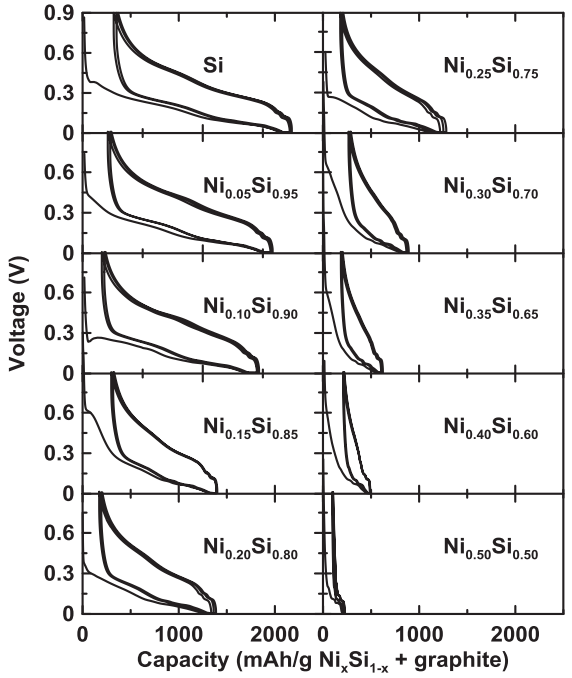

Figure 4. Voltage curves of Ni–Si alloy–graphite composite electrodes, the compositions of the Ni_xSi_{1-x} alloys is indicated in each panel.

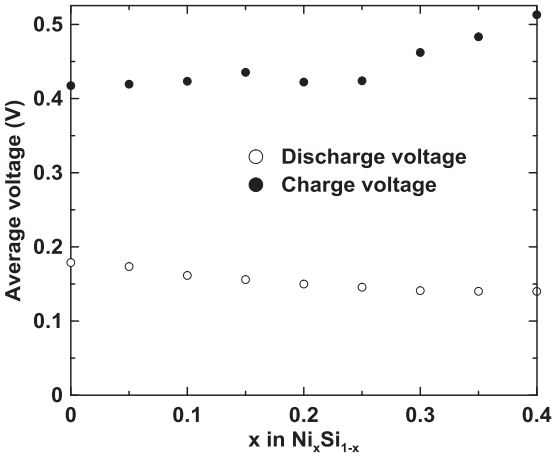

Figure 5. Average second lithiation and delithiation voltage of Ni_xSi_{1-x} alloys versus x, as calculated by subtracting the graphite contribution from the voltage curves in Figure 4.

increase afterwards. This trend for the ball milled Ni-Si alloys is very similar to that observed for sputtered Ni-Si thin films.[7] The voltage depression during lithiation avoids $Li_{15}Si_4$ crystalline phase formation (as discussed below), while the unchanged delithiation voltage would not impair the discharge potential of a full Li-ion battery.

Figure 6 shows differential capacity curves for the 1st (black line), 2nd (black line), 10th (blue line) and 20th (red line) cycles of Ni–Si alloy–graphite composite electrodes described in Figure 4. For the 1st

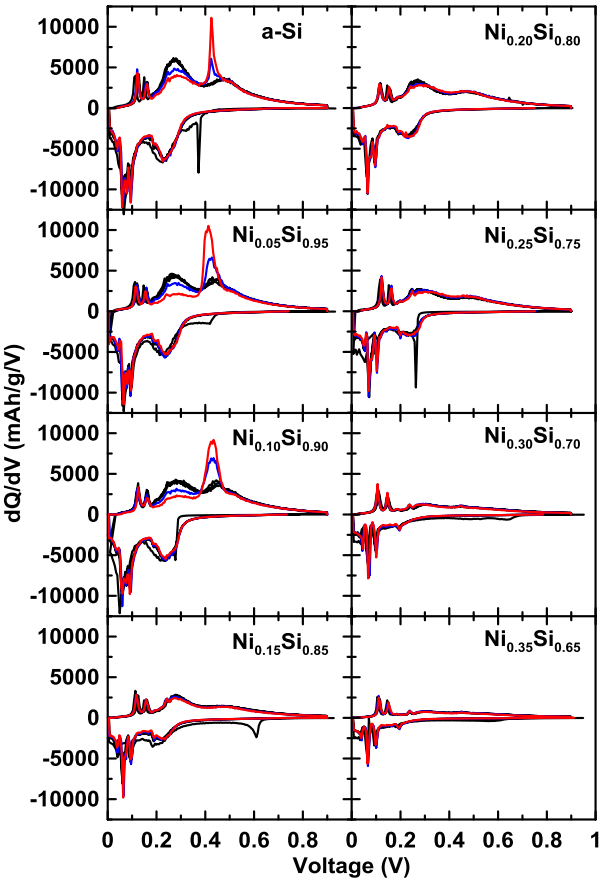

Figure 6. Differential capacity curves of Ni–Si alloy–graphite composite electrodes derived from Figure 4 for the 1st, 2nd (both black), 10th (blue) and 20th (red) cycles.

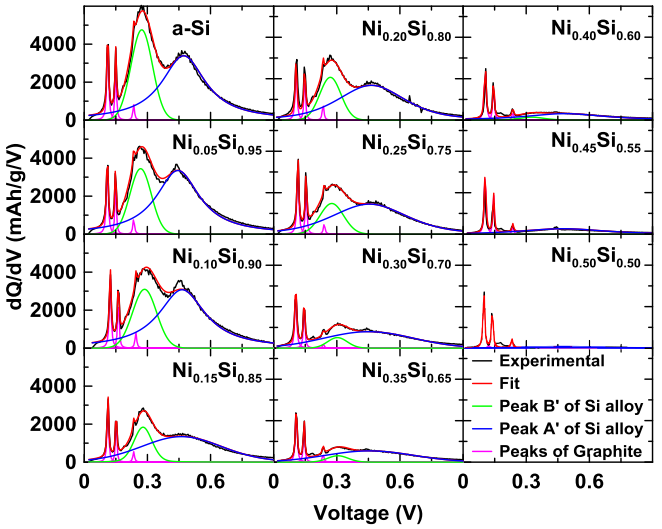

Figure 7. Pseudo-Voigt fits of the differential capacity curve peaks during the first delithiation.

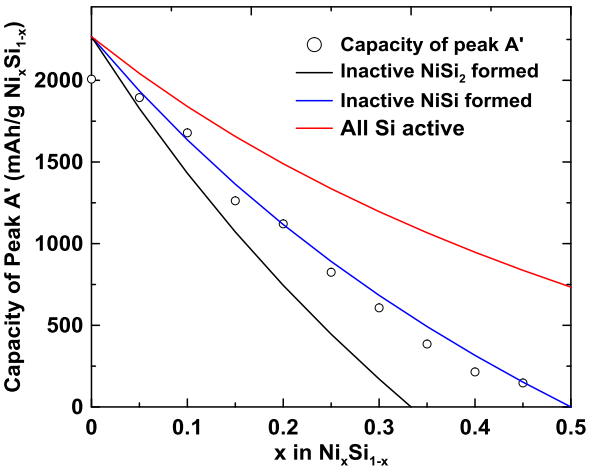

Figure 8. Delithiation capacity as measured from the differential capacity peak A′ of Ni_xSi_{1-x} alloys calculated from the fits in Figure 7.

and 2nd cycles, all electrodes show the features of broad peaks from amorphous Si alloys and sharp peaks from graphite. The enclosed area of the differential capacity curves gradually decreases with increasing Ni, corresponding to the decreasing capacity in Figure 4. With increasing cycle number, electrodes containing amorphous Si (a-Si), $Ni_{0.05}Si_{0.95}$ and $Ni_{0.10}Si_{0.90}$ alloys form a sharp peak at around 0.42 V during charge, indicating the occurrence of a two-phase transition between crystalline $Li_{15}Si_4$ and Si. This peak is broader for the $Ni_{0.05}Si_{0.95}$ and $Ni_{0.10}Si_{0.90}$ samples than that for pure Si sample. We speculate that this may be caused by the presence of Ni, either by the modification of the $Li_{15}Si_4$ chemistry or by intra-particle stress due to the presence of an inactive phase.

For electrodes with $x \geq 0.15$, the differential capacity curves remain unchanged during cycling, indicating that no $Li_{15}Si_4$ phase is formed in these cells. Obrovac et al. reported that the crystalline $Li_{15}Si_4$ phase can be avoided in pure Si by limiting lithiation voltage to above 50 mV.[3] In the present study, since the lithiation voltage is already depressed by increasing Ni, $Li_{15}Si_4$ phase is avoided even though electrodes are discharged to 5 mV. This behavior is the same as we have previously reported for the suppression of $Li_{15}Si_4$ formation in sputtered Ni-Si films.[7]

As discussed in Reference 6, to accurately determine the amount of active Si, the shift in the voltage curve must be taken into account. Since peaks A/A′ remain above 0 V, despite the voltage shift, they may be used to estimate the amount of active Si present. Peak fitting of the differential capacity curves during the first delithiation half-cycle is shown in Figure 7 and capacity corresponding to peak A′ is plotted in Figure 8 versus composition. Peak A' was found to have a capacity of 2267 mAh/g for sputtered $Ni_{0.04}Si_{0.96}$ thin film and this was used as the maximum capacity when $x = 0$ on which to base the calculations.[7] Three calculated models are shown in Figure 8: the theoretical capacity assuming all the Si is active, the theoretical capacity assuming inactive $NiSi_2$ is formed and the remaining elemental Si is active or the theoretical capacity assuming inactive NiSi is formed and the remaining elemental Si is active.

According to the XRD results in Figure 1, which indicate Si-$NiSi_2$ two-phase coexistence, the capacity of peak A′ should follow the black line, if $NiSi_2$ is inactive for $x < 0.30$. The peak A′ capacities of Ni_xSi_{1-x} alloys do gradually decrease with increasing x. However, the experimental data is not consistent with the presence of inactive $NiSi_2$. Instead, the data follows the line corresponding to the presence of inactive NiSi quite closely. This suggests that the $NiSi_2$ phase in ball milled Si/$NiSi_2$ alloys, as formed here for $x < 0.3$, is active during lithiation/delithiation and that during lithiation inactive NiSi is formed, according to the formula:

$$Si/NiSi_2 + yLi \rightarrow 2Li_{y/2}Si + NiSi \quad [1]$$

According to previous reports,[11,18,26] a capacity of about 200 mAh/g was observed for $NiSi_2$ and the value can be as high as ~600 mAh/g for nanocrystalline $NiSi_2$. We have confirmed that nanocrystalline $NiSi_2$ phase made by ball milling is indeed active. These results will be presented in another study.[27] This behavior of ball milled Ni-Si alloys differs from the results of Ni-Si thin films, in which Ni was found to be the inactive phase.[7]

In situ XRD was used to further clarify the mechanism that occurs during the cycling of ball milled Ni-Si alloy powders. Figure 9 shows the in-situ XRD patterns of the $Ni_{0.25}Si_{0.75}$ sample at different discharge/charge states. The patterns are offset from each other by 200 counts for clarity. A high intensity sharp peak between 45° and 46° from cell parts was removed from all the XRD patterns in

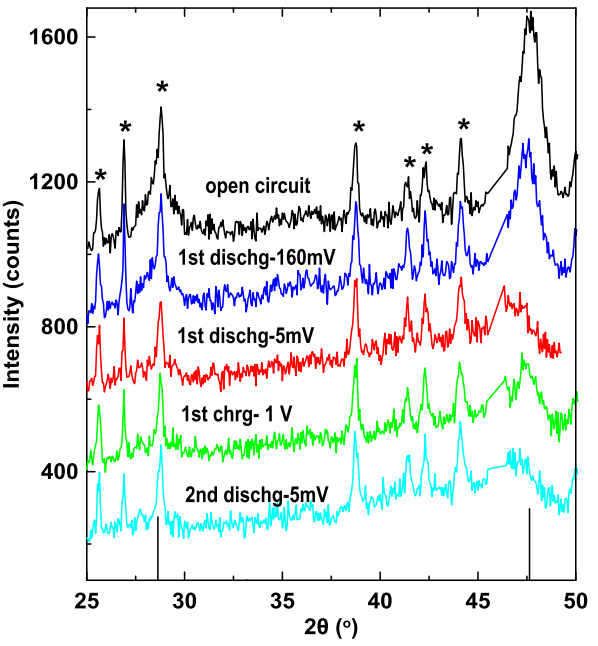

Figure 9. In situ XRD patterns of $Ni_{0.25}Si_{0.75}$ during lithiation and delithiation. The state of charge is indicated in the figure. Diffraction peaks from $NiSi_2$ are indicated with black vertical lines at 28.6° and 47.6°. All other sharp peaks originate from cell parts and are marked with asterisks.

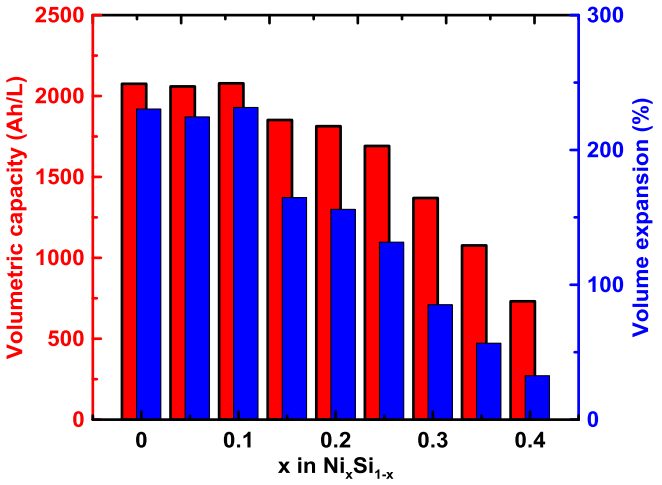

Figure 10. Volumetric capacity and volume expansion of ball milled Ni_xSi_{1-x} alloys versus x.

the figure for clarity. Diffraction peaks from $NiSi_2$ are indicated with black vertical lines at 28.6° and 47.6° 2-theta. All other sharp peaks originate from cell parts and are marked with asterisks. During the first lithiation, the intensity of the $NiSi_2$ peaks gradually decreases, indicating that $NiSi_2$ and Li react to make an amorphous product. This provides further confirmation of the activity of $NiSi_2$, suggested in Equation 1, where the inactive NiSi formed is amorphous. During the subsequent delithiation the $NiSi_2$ peaks do not reappear. Either $NiSi_2$ is not reformed during delithiation or it is amorphous.

Figure 10 shows the volumetric capacities and volume expansions of Ni_xSi_{1-x} alloys based on a calculation of 9 mL/mol of Li in Si-based materials.[1] Both volumetric capacity and volume expansion are reduced with increasing x, as expected. The improvement in energy density from utilizing alloy electrodes can be estimated by using a cell stack model.[2] In this study, no appreciable improvement in stack energy density can be obtained for $x \geq 0.30$ because the volumetric capacity is low. For $x \leq 0.15$, the volume expansion is over 200% and these alloys also suffer from $Li_{15}Si_4$ formation during cycling. Thus, a reasonable composition range for Ni-Si alloys may be $0.15 < x < 0.3$ in Ni_xSi_{1-x}. Such alloys can have volumetric capacities between 1370 Ah/L and 1823 Ah/L and are calculated to improve the energy density of a cell stack by up to 23% - 30% over graphite electrodes according to a cell stack model.[2]

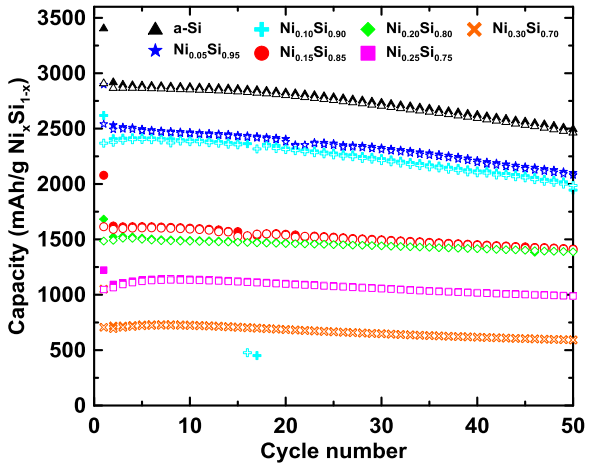

Figure 11. The lithiation (closed symbols) and delithiation (open symbols) capacities of ball milled Ni_xSi_{1-x} alloys versus cycle number.

Figure 11 shows the specific capacity of Ni_xSi_{1-x} alloys versus cycle number obtained from Ni–Si alloy–graphite composite electrodes. For $x \leq 0.2$, cycling performance is improved with increasing x, with the best cycling performance obtained for the $Ni_{0.20}Si_{0.80}$ sample. This is attributed to the reduced volume expansion, as shown in Figure 10, and the absence of $Li_{15}Si_4$ phase formation, as indicated in Figure 6. With the further increases in x, the capacity retention is not improved and all of the samples show a similar linear fade. The capacity retention for the $Ni_{0.20}Si_{0.80}$-graphite composite electrode is 94% of the initial delithiation capacity after 50 cycles. This electrode would provide about 14% improvement over graphite when incorporated in a Li-ion cell, according to the cell stack model in Reference 2. However, cycle life needs to be improved further for use in practical applications.

Conclusions

Ni_xSi_{1-x} alloys over a large region of compositions ($0 \leq x \leq 0.5$) were prepared by ball milling. XRD patterns showed that nanostructured Si/$NiSi_2$ alloys were formed for $x \leq 0.25$ and NiSi was formed with further increase of x. All the alloys have voltage curves typical for that of amorphous Si for the first several cycles, however the lithiation voltage was gradually depressed with increasing x, while delithiation showed little change for $x \leq 0.25$. This is similar to the behavior of Ni-Si thin film and is indicative of internal particle stress during lithiation. The lithiation voltage depression resulted in the elimination of $Li_{15}Si_4$ formation during cycling for $x \geq 0.15$, which coincided with improved cycling performance.

It was found that the voltage/capacity behavior of the Ni-Si alloys corresponds to the presence of inactive NiSi in the cycled alloy. This is different than what is observed in Ni-Si sputtered films, in which Ni was found to be the inactive phase. It is concluded that the nanocrystalline $NiSi_2$ phase in ball milled Ni-Si alloys is active during lithiation/delithiation, while the NiSi phase was completely inactive. Good cycling retention was obtained for Si contents up to 80%, with a capacity retention of 94% was obtained for the $Ni_{0.20}Si_{0.80}$ alloy after 50 cycles. This composition has a volumetric capacity of about 1350 Ah/L. Cycle life must be improved further for use in practical cells.

Acknowledgments

The authors acknowledge funding from NSERC and 3 M Canada, Co. under the auspices of the Industrial Research Chair program. We also acknowledge the support of the Canada Foundation for Innovation, the Atlantic Innovation Fund and other partners that fund the Facilities for Materials Characterization managed by the Institute for Research in Materials. ZD acknowledges financial support from the Killam Trusts.

References

1. M. N. Obrovac, L. Christensen, Dinh Ba Le, and J. R. Dahn, *J. Electrochem. Soc.*, **154**, A849 (2007).
2. M. N. Obrovac and V. L. Chevrier, *Chem. Rev.*, **114**(23), 11444 (2014).
3. M. N. Obrovac and L. Christensen, *Electrochem. Solid-State Lett.*, **7**, A93 (2004).
4. L. Y. Beaulieu, T. D. Hatchard, A. Bonakdarpour, M. D. Fleischauer, and J. R. Dahn, *J. Electrochem. Soc.*, **150**, A1457 (2003).
5. M. T. McDowell, S. W. Lee, W. D. Nix, and Y. Cui, *Adv. Mater.*, **25**, 4966 (2013).
6. X. H. Liu and J. Y. Huang, *Energy Environ. Sci.*, **4**, 3844 (2011).
7. Z. Du, T. D. Hatchard, R. A. Dunlap, and M. N. Obrovac, *J. Electrochem. Soc.*, **162**, A1858 (2015).
8. V. L. Chevrier, L. Liu, D. B. Le, J. Lund, B. Molla, K. Reimer, L. J. Krause, L. D. Jensen, E. Figgemeier, and K. W. Eberman, *J. Electrochem. Soc.*, **161**, A783 (2014).
9. Z. Du, R. A. Dunlap, and M. N. Obrovac, *J. Electrochem. Soc.*, **161**, A1698 (2014).
10. S Kirklin, B Meredig, and C Wolverton, *Adv. Energy Mater.*, **3**, 252 (2013).
11. A. Netz, R. A. Huggins, and W. Weppner, *J. Power Sources*, **119**, 95 (2003).
12. H. Usui, K. Meabara, K. Nakai, and H. Sakaguchi, *Int. J. Electrochem. Sci.*, **6**, 2246 (2011).
13. H.-Y. Lee and S.-M. Lee, *J. Power Sources*, **112**, 649 (2002).
14. M.-S. Park, Y.-J. Lee, S. Rajendran, M.-S. Song, H.-S. Kim, and J.-Y. Lee, *Electrochim. Acta*, **50**(28), 5561 (2005).
15. Y. S. Lee, J. H. Lee, Y. W. Kim, Y. K. Sun, and S. M. Lee, *Electrochim. Acta*, **52**, 1523 (2006).

16. M. D. Fleischauer, J. M. Topple, and J. R. Dahn, *Electrochem. Solid-State Lett*, **8**(2), A137 (2005).
17. M D. Fleischauer, R. Mar, and J. R. Dahn, *J. Electrochem. Soc.*, **154**(3), A151 (2007).
18. M. J. Kim, D. G. Kim, and H.-J. Sohn, NiSi2 Alloy as an Anode Materials for Lithium-ion Batteries, *202nd Meeting of the Electrochemical Society*, 2002, Abstract #18.
19. G. X. Wang, L. Sun, D. H. Bradhurst, S. Zhong, S. X. Dou, and H. K. Liu, *J. Power Sources*, **88**, 278 (2000).
20. Y.-N. Zhou, W.-J. Li, H.-J. Chen, C. Liu, L. Zhang, and Z. Fu, *Electrochem. Comm.*, **13**(6), 546 (2011).
21. W.-R. Liu, N.-L. Wu, D.-T. Shieh, H.-C. Wu, M.-H. Yang, C. Korepp, J. O. Besenhard, and M. Winter, *J. Electrochem. Soc.*, **154**(2), A97 (2007).
22. V. A. Sethuraman, V. Srinivasan, A. F. Bower, and P. R. Guduru, *J. Electrochem. Soc.*, **157**(11), A1253 (2010).
23. P. P. Ferguson, Dinh-Ba Le, A. D. W. Todd, M. L. Martine, S. Trussler, M. N. Obrovac, and J. R. Dahn, *J. Alloys Compd.*, **595**, 138 (2014).
24. M. N. Richard, I. Koetschau, and J. R. Dahn, *J. Electrochem. Soc.*, **144**(2), 554 (1997).
25. International Centre for Diffraction Data PDF-2, Release 2002.
26. Z. Wen, S. Ji, J. Sun, F. Tian, R. Tian, and J. Xie, *Rare Metals*, **25**, 77 (2006).
27. Z. Du, P. Bissonnette, T. D. Hatchard, R. A. Dunlap, and M. N. Obrovac, *in preparation*.